Reduction of interfacial thermal resistance of overlapped graphene by bonding carbon chains

Yuwen Huang(黄钰文)[1,2], Wentao Feng(冯文韬)[1,2], Xiaoxiang Yu(余晓翔)[1,2], Chengcheng Deng(邓程程)[1,†], and Nuo Yang(杨诺)[1,2,‡]

Citation: Chin. Phys. B, 2020, 29 (**12**): 126303. DOI: 10.1088/1674-1056/abc677
Journal homepage: http://cpb.iphy.ac.cn; http://iopscience.iop.org/cpb

What follows is a list of articles you may be interested in

Reduction of interfacial thermal resistance of overlapped graphene by bonding carbon chains

Yuwen Huang(黄钰文)[1,2], Wentao Feng(冯文韬)[1,2], Xiaoxiang Yu(余晓翔)[1,2], Chengcheng Deng(邓程程)[1,†], and Nuo Yang(杨诺)[1,2,‡]
Chin. Phys. B, 2020, 29 (**12**): 126303. DOI: 10.1088/1674-1056/abc677

Surface-regulated triangular borophene as Dirac-like materials from density functional calculation investigation

Wenyu Fang(方文玉), Wenbin Kang(康文斌), Jun Zhao(赵军), Pengcheng Zhang(张鹏程)
Chin. Phys. B, 2020, 29 (**9**): 096301. DOI: 10.1088/1674-1056/ab9bff

Multilayer graphene refractive index tuning by optical power

Lijun Li(李丽君), Yilin Liu(刘仪琳), Yinming Liu(刘荫明), Lin Xu(徐琳), Fei Yu(于飞), Tianzong Xu(徐天纵), Zhihui Shi(石志辉), Weikang Jia(贾伟康)
Chin. Phys. B, 2018, 27 (**12**): 126304. DOI: 10.1088/1674-1056/27/12/126304

Thermal transport in semiconductor nanostructures, graphene, and related two-dimensional materials

Alexandr I. Cocemasov, Calina I. Isacova, Denis L. Nika
Chin. Phys. B, 2018, 27 (**5**): 056301. DOI: 10.1088/1674-1056/27/5/056301

Two-dimensional arsenic monolayer sheet predicted from first-principles

Pu Chun-Ying, Ye Xiao-Tao, Jiang Hua-Long, Zhang Fei-Wu, Lu Zhi-Wen, He Jun-Bao, Zhou Da-Wei
Chin. Phys. B, 2015, 24 (**3**): 036301. DOI: 10.1088/1674-1056/24/3/036301

SPECIAL TOPIC — Phononics and phonon engineering

Reduction of interfacial thermal resistance of overlapped graphene by bonding carbon chains*

Yuwen Huang(黄钰文)[1,2], Wentao Feng(冯文韬)[1,2], Xiaoxiang Yu(余晓翔)[1,2], Chengcheng Deng(邓程程)[1,†], and Nuo Yang(杨诺)[1,2,‡]

[1] School of Energy and Power Engineering, Huazhong University of Science and Technology, Wuhan 430074, China
[2] State Key Laboratory of Coal Combustion, Huazhong University of Science and Technology, Wuhan 430074, China

(Received 20 September 2020; revised manuscript received 29 October 2020; accepted manuscript online 31 October 2020)

Exploring the mechanism of interfacial thermal transport and reducing the interfacial thermal resistance are of great importance for thermal management and modulation. Herein, the interfacial thermal resistance between overlapped graphene nanoribbons is largely reduced by adding bonded carbon chains as shown by molecular dynamics simulations. And the analytical model (phonon weak couplings model, PWCM) is utilized to analyze and explain the two-dimensional thermal transport mechanism at the cross-interface. An order of magnitude reduction of the interfacial thermal resistance is found as the graphene nanoribbons are bonded by just one carbon chain. Interestingly, the decreasing rate of the interfacial thermal resistance slows down gradually with the increasing number of carbon chains, which can be explained by the proposed theoretical relationship based on analytical model. Moreover, by the comparison of PWCM and the traditional simplified model, the accuracy of PWCM is demonstrated in the overlapped graphene nanoribbons. This work provides a new way to improve the interfacial thermal transport and reveal the essential mechanism for low-dimensional materials applied in thermal management.

Keywords: phonon engineering, graphene, phonon weak couplings model, molecular dynamics

PACS: 63.22.Rc, 65.80.Ck, 05.70.Np, 31.15.xv **DOI:** 10.1088/1674-1056/abc677

1. Introduction

Nowadays, low-dimensional materials have aroused widespread research interest and show great application prospects.[1–4] Representatively, graphene, a two-dimensional nanomaterial composed of carbon atoms with sp^2 hybrid orbital hexagonal honeycomb lattice, has received continuous attention due to its many intriguing characteristics, such as superior thermal conductivity,[5–9] strong mechanical strength,[10,11] electronic properties,[12–16] and optical transparency.[17–19] In particular, due to the superior thermal conductivity (exceeding $\sim$ 3000 W/K·m near room temperature[6]), graphene plays a growing significant role in the thermal management of the next generation electronic devices.[20–25] As a two-dimensional material, graphene has a remarkable characteristic, that is anisotropic heat flows in two directions: in-plane and out-of-plane. Covalent sp^2 bonding between the carbon atoms leads to a high in-plane thermal conductivity, whereas the out-of-plane heat flow is limited by weak van der Waals coupling.[26]

As an excellent material with high in-plane thermal conductivity, graphene is usually applied in various ways for heat dissipation.[27,28] For example, graphene is used as a filler to synthesize organic compounds into polymer, which optimizes the thermal properties of the organic compounds and serves as a thermal interface material.[29–32] Besides, it is arranged in an orderly stack to synthesize macro-scale films with high thermal conductivity for use as a heat dissipation substrate.[33,34] In practical applications, however, these methods cannot greatly increase the thermal conductivity of the materials. The reason is that there are lots of interfaces between the organic substance and graphene or between graphene and graphene.[35,36] These interfaces usually have large thermal resistances, which significantly affects the thermal transport in the composite system.[37] Therefore, it is necessary to investigate the interfacial thermal transport of the graphene-based composites.

There are a large number of nano-scale interfaces observed in composites and films.[38–41] The low-dimensional materials, like graphene,[42] carbon nanotube (CNT), and boron nitride (BN),[39] are staggered in parallel and form many overlapped interfaces, which are called as cross-interfaces. Different from the unidirectional heat conduction phenomenon at the traditional interface, when the heat flows through this interface, it is simultaneously transported inside and between the ribbons, forming a two-dimensional heat conduction process.[43–46] To reduce the thermal resis-

*Project supported by the National Natural Science Foundation of China (Grant No. 51606072) and the Fundamental Research Funds for the Central Universities, HUST, China (Grant No. 2019kfyRCPY045).

†Corresponding author. E-mail: dengcc@hust.edu.cn
‡Corresponding author. E-mail: nuo@hust.edu.cn

tance of cross-interface of low-dimensional materials, several methods have been adopted in experimental and simulation works.[47–49] For instance, Qiu *et al.*[50] promoted interfacial thermal transport by using the intriguing CNT fibers decorated with Au nanoparticles as a promising platform. Liu *et al.*[51] found that the junctions formed by $-C_2H_4-$ molecular groups between two graphene nanoribbons (GNRs) are effective for transmitting the out-of-plane phonon modes of GNRs. In Xu *et al.*'s work,[52] polymer wrapping significantly improved the interfacial thermal conductivity of the CNT interfaces. The polymer chains were lying along the groove between CNTs when the wrapping density was assured and assisted the heat transfer process. In this work, a new and simple method is proposed to reduce the interfacial thermal resistance by adding carbon chains bonded between the overlapped graphene nanoribbons.

In previous works, thermal transport at cross-interface was traditionally treated by point contact or by approximation methods. For instance, Yang *et al.* treated the total thermal resistance of the cross-interface as the sum of the interfacial thermal resistances and the in-plane thermal resistance with half of the overlapping length in series[53,54] (i.e., simplified model, SM). Zhong *et al.* calculated the interfacial thermal resistance by treating the overlapped region as a single planar interface between coaxial hot and cold nanotubes joined end to end.[55] Liu *et al.* calculated the total thermal conductance of the overlapped region based on the Fourier law, where the temperature difference was given by the average temperature difference.[51] In experimental works, the total thermal resistance of a cross-interfacial sample was usually firstly measured by using a thermal bridge method,[56,57] then one segment was removed and the other was realigned to bridge the two membranes. From these two measurements, the interfacial thermal resistance could be extracted.[54] Generally, these methods approximately treated the interface system as one-dimensional thermal transport process and lacked the accurate mechanism exploration of thermal transport at the cross-interface. Recently, an analytical model, named as the phonon weak couplings model (PWCM),[58] has been proposed to explore the mechanism of the two-dimensional thermal transport, which is classified as implicit couplings and explicit couplings. The model of explicit coupling focuses on the cross-interface, and is also named as the cross-interface model (CIM).[59,60]

In this work, the interfacial thermal resistance at the cross-interface between two overlapped graphene nanoribbons is effectively reduced through bonding carbon chains (CCs), and the theoretical model of PWCM is applied to analyze and explain the physical mechanism of thermal transport at the cross-interface. Firstly, the basic idea and framework of the PWCM theoretical model are presented and molecular dynamics simulation is carried out to calculate the interfacial thermal resistance of two overlapped graphene nanoribbons. Then, the PWCM is applied to analyze and explain the interfacial thermal resistances of the overlapped graphene nanoribbons, and the influence of CCs' number on the thermal transport is investigated. Lastly, the advantage of PWCM relative to the traditional SM for thermal transport at the cross-interface is compared and discussed. Our study not only provides a new way to improve the interfacial thermal transport of graphene-based composites, but also deepens the understanding of the thermal transport at the cross-interfaces.

2. Theoretical model and simulation method

2.1. Phonon weak couplings model

The PWCM is utilized to calculate and analyze the thermal transport in the overlapped graphene nanoribbons. Here, PWCM is derived on the base of Boltzmann transport equation (BTE). There is size effect in micro/nanoscale phonon transport when the size of the structures is comparable to the mean free path of phonons. For classical size effects which do not consider the quantum effect, the phonon transport is greatly affected by boundary scatterings. Transport processes with classical size effects can be treated on the basis of BTE by treating the phonons as particles.[61] Moreover, from Ma *et al.*'s work, it can be seen that the particle characteristics of phonon transport still exist widely in the nanoscale materials.[62] Therefore, It is worth to note that BTE is not only applicable to diffusive transport, but also suitable for ballistic transport under certain conditions.[61]

For such a cross-interface, the heat flows along the structure horizontally and through the interface vertically simultaneously. The PWCM is applicable to illustrate the two-dimensional thermal transport process at the cross-interface by considering the coupling effect between different thermal transport channels. The coupling effects may be much weaker than the phonon transport in each ribbon, but it is not negligible for the thermal transport in the entire system. Referring to the works of Feng *et al.*,[60] Xiong *et al.*,[59] and Deng *et al.*,[58] the PWCM is based on Fourier's law and energy conservation. In the overlapped region, the heat conduction equations for each ribbon are given below:

$$\kappa \frac{\mathrm{d}^2 T_\mathrm{T}}{\mathrm{d}x^2} A - G_\mathrm{CA}\left(T_\mathrm{T} - T_\mathrm{B}\right) w = 0, \quad 0 < x < L_\mathrm{C}, \tag{1a}$$

$$\kappa \frac{\mathrm{d}^2 T_\mathrm{B}}{\mathrm{d}x^2} A + G_\mathrm{CA}\left(T_\mathrm{T} - T_\mathrm{B}\right) w = 0, \quad 0 < x < L_\mathrm{C}, \tag{1b}$$

where T_T and T_B are the temperatures of the top and bottle GNRs, respectively. w is the width of the GNRs and A is the cross sectional area. G_CA is the interfacial thermal conductance per unit area and κ is the thermal conductivity of the two same GNRs. L_C is the length of the overlapped region.

Through a series of formula conversions,[60] the temperature distribution functions can be obtained as follows:

$$T_{\mathrm{T}} = \frac{1}{2}(a \times \mathrm{e}^{-\gamma x} + b \times \mathrm{e}^{\gamma x} + cx + d), \tag{2a}$$

$$T_{\mathrm{B}} = \frac{1}{2}(-a \times \mathrm{e}^{-\gamma x} - b \times \mathrm{e}^{\gamma x} + cx + d), \tag{2b}$$

$$\gamma = \sqrt{2G_{\mathrm{CA}}w/\kappa A}, \tag{3}$$

where a, b, c, d are parameters and the details are shown in the supporting information. The thermal resistance can be deduced as follows:

$$R_{\mathrm{total}} = R_{\mathrm{intra}} + \frac{1}{\eta} \times R_{\mathrm{inter}}, \tag{4}$$

$$\eta = \frac{\tanh\sqrt{R_{\mathrm{intra}}/R_{\mathrm{inter}}}}{\sqrt{R_{\mathrm{intra}}/R_{\mathrm{inter}}}}, \tag{5}$$

where R_{total} is the total thermal resistance; R_{intra} is the intra-ribbon thermal resistance assuming that the top ribbon and the bottom ribbon transport heat in a parallel mode, just like the parallel law in electrical transport; R_{inter} is the inter-ribbon thermal resistance, which is the inverse of the interfacial thermal conductance. And η is a factor related to the ratio of R_{intra} and R_{inter}. The detailed explanation of the formula is shown in the supporting information.

2.2. MD simulation method

In this work, the nonequilibrium molecular dynamics (NEMD) is utilized to calculate the interfacial thermal resistance between two overlapped GNRs.[63–65] The simulation system consists of two same GNRs, which are overlapped in z direction as shown in Fig. 1. Each GNR is 10.19 nm long and 3.05 nm wide, and the length of the overlapped region (L_{C}) is 9.21 nm. The interlayer distance between the two GNRs is 0.35 nm. Different numbers of carbon chains (CC), including 1, 3, 5, and 7, are respectively bonded between the two GNRs cross the overlapped section. The carbon atoms in the CC are connected alternately by single and double bonds; the CC and GNR are bonded by sp^3 bonds. The three bonds on each atom of CC are distributed in the same plane and the bond angles are all 120° initially. The CCs are evenly distributed in the width direction of GNR. In order to ensure that the atomic layers at both ends of the overlapped-GNRs are connected by CCs, adjacent CCs are staggered by a C–C bond horizontal distance (L_{o} in Fig. 1(d)) in the z direction.

In the MD simulations herein, the Tersoff potential is employed to describe the interatomic interactions, while it has successfully tested the thermal conductivity of GNR[64,66] and the thermal properties of graphene.[63,67,68] The van der Waals interactions between the two GNRs are described by the Lenard–Jones (L–J) potential,[52] $V_{ij} = 4\varepsilon[(\sigma/r)^{12} - (\sigma/r)^6]$, $\varepsilon = 0.002968$ eV, $\sigma = 3.407$ Å, where ε is the depth of the potential energy well, σ is the finite distance at which the interatomic potential is zero, and r is the distance between the atoms. The time step of all simulations is set as 0.25 fs, and the velocity Verlet algorithm is used to integrate the discrete differential equations of motion.[69]

All the simulations here are performed by the large-scale atomic/molecular massively parallel simulator (LAMMPS) packages,[70] which have been widely used to study thermal transport properties at nanoscale.[71–73] In the simulation structure, the size of the simulation box is $10 \times 10 \times 19.65$ nm^3, which is much larger than the initial volume of the overlapped graphene. The GNR structure is firstly equilibrated at a constant temperature for 250 ps in the canonical ensemble (NVT) and then in the microcanonical ensemble (NVE) for 100 ps. Then a layer of atoms at both ends of the structure is fixed (yellow region in Fig. 1). Afterwards, a heat source with a higher temperature of 320 K is applied to the atoms in the red region and a heat sink with a lower temperature of 280 K is applied to atoms in the blue region using Langevin thermostats. After the system reaches the steady state by performing simulation for 2.5 ns, time averaging of temperature and heat current is performed for an additional 25 ns to get the temperature profile and the heat flux (NEMD simulation details are given in the supplementary material). And the reliability of the simulation method is verified by calculating the thermal conductivity of the GNR sheets, which is consistent with that in previous works[74] (related calculation details are shown in the supplementary material).

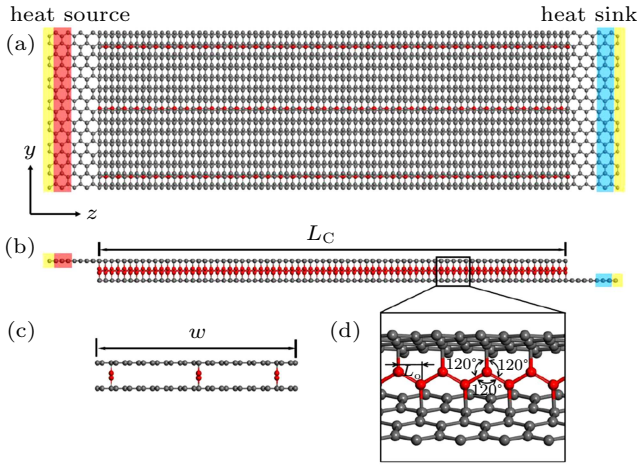

Fig. 1. Schematic of two overlapped graphene nanoribbons bonded by three carbon chains: (a) top view; (b) front view; (c) side view; (d) the local enlarged drawing of bonded carbon chains (red chains) between the two graphene nanoribbons.

3. Results and discussion

Firstly, NEMD method is performed to obtain the temperature profile of the structures, then equation (1) in the PWCM theoretical model is used to fit the calculation results in the overlapped section. A typical temperature profile of the interface structure bonded by three CCs is presented in Fig. 2(a). It

is seen that the results are fitted fairly well by using the PWCM (the red line). And the coefficient of determination (R^2) is equal to 0.99829, which exhibits the good fitting quality.

Three kinds of thermal resistances are obtained through the calculations. As shown in Fig. 2(b), with the number of CCs increasing, the total thermal resistance (R_{total}) and inter-ribbon thermal resistance (R_{inter}) decrease significantly, and the intra-ribbon thermal resistance (R_{intra}) increases slowly. When no CC is bonded, the interfacial thermal resistance is very large because the van der Waals interaction between the two graphene ribbons is extremely weak. The R_{total} and R_{inter} for the case with no CC are equal to 7.27×10^8 K/W and 7.20×10^8 K/W, respectively. After one CC is bonded, the R_{total} and R_{inter} are 9.25×10^7 K/W and 7.40×10^7 K/W, respectively, which are nearly one order of magnitude lower than those in the case with no CC. It is confirmed that covalent bond interactions dominate in the interfacial thermal transport which are much stronger than the van der Waals interactions. It is noteworthy that when the number of CCs increases to three, the thermal resistance tends to converge. This reason will be discussed later. Moreover, the values of R_{intra} basically keep the same when the number of CCs increases from one. This indicates that the thermal conductivity of the GNR remains unchanged with the increasing number of CC bonded in the out-plane direction.

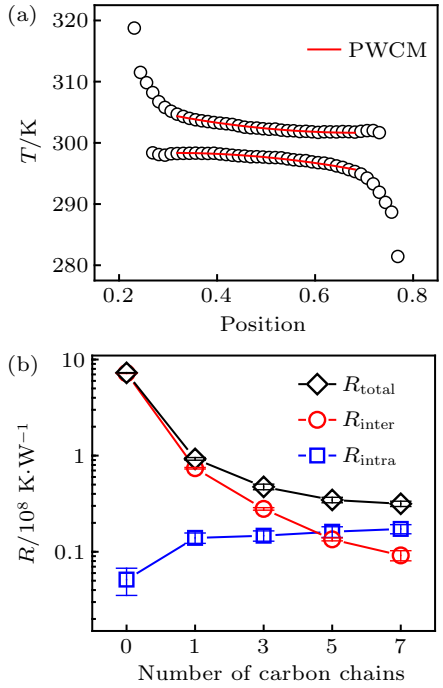

Fig. 2. (a) Temperature profile of overlapped graphene nanoribbons bonded by three carbon chains. The temperature distribution using PWCM can fit to the simulation result as the red line. (b) Influence of the number of carbon chains on thermal resistance at the cross-interface.

The variation of the interfacial thermal conductance per unit area (G_{CA}) with the number of CCs is depicted in Fig. 3(a). When no CC is bonded, the value of G_{CA} is 6.39×10^7 W/K·m^2. After one CC is bonded, the value rises to 6.22×10^8W/K·m^2, which is nearly one order of magnitude higher. It is confirmed again that covalent bond interactions greatly enhance the interfacial thermal conductance. More interestingly, the interfacial thermal conductance per unit area nearly follows a linear relationship with the number of CCs (shown as blue line in Fig. 3(a)). This indicates that each CC serves as an independent channel for heat conduction, and there is little coupling between adjacent CCs.

It can be seen from Fig. 2(b) that the decreasing rate of R_{inter} slows down gradually with the increasing number of boned CCs. In order to analyze this tendency theoretically, G_{CA} is considered to contain two parts: one is devoted by van der Waals interactions and the other is contributed by covalent bond interactions. Based on these assumptions and analysis, the interfacial thermal conductance per unit area can be given by

$$G_{\text{CA}} = N \cdot \Delta G + G_0, \tag{6}$$

where ΔG represents the interfacial thermal conductance per unit area that each CC possesses and N represents the number of CCs. Here, when $N = 0$ for the case without bond-chain, $G_{\text{CA}} = G_0$. Therefore, G_0 represents the interfacial thermal conductance per unit area in the case without bond-chain.

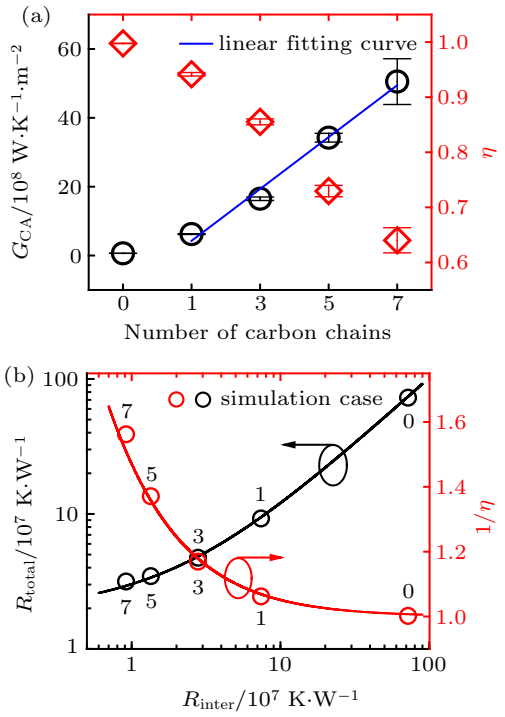

Fig. 3. (a) Interfacial thermal conductance per unit area (black hollow dot) and dimensionless factor η (red hollow diamond) as a function of the number of carbon chains. Blue line is the linear fitting line from NEMD results. (b) R_{total} (black line) and $1/\eta$ (red line) as a function of R_{inter}. The hollow dots show the five simulation results, and the Arabic numerals represent the number of carbon chains.

According to Eq. (6), R_{inter} can be derived as

$$R_{\text{inter}} = \frac{1}{wL_{\text{C}} \cdot \sqrt{(N \cdot \Delta G + G_0)}}. \tag{7}$$

It can be noted that there is a roughly proportional relationship ($R_{\text{inter}} \propto 1/\sqrt{N}$) in Eq. (7). Therefore, when N further increases, the decreasing rate of R_{inter} slows down and R_{inter} tends to numerical convergence.

Furthermore, the relationship curve of R_{total} and R_{inter} is given in Fig. 3(b). Herein, the R_{intra} is regarded as a constant in Eq. (4) because it represents the intrinsic thermal resistance of the GNR and the calculation results in Fig. 2(b) basically keep the same when the number of CCs increases from one. The results show that when CCs' number increases (R_{inter} decreases), R_{total} decreases monotonically. Since η is a coefficient related to R_{inter} according to Eq. (5), the relationship curve of $1/\eta$ and R_{inter} is shown as the red line in Fig. 3(b). Although $1/\eta$ increases to infinity when R_{inter} decreases, it cannot change the monotonically decreasing trend of R_{total}. This can be theoretically explained by that increasing the number of CCs in the overlapped area significantly reduces the thermal resistance of the overlapped graphene. Moreover, the simulation results of five cases are depicted as hollow dots in Fig. 3(b). These simulation dots fall well on the theoretical curve, which confirms the accuracy of the PWCM.

To compare between the PWCM and traditional SM, the theoretical curves of temperature distribution using PWCM and SM are shown in Fig. 4(a). The solid exponential curve in the overlapped region is drawn with Eq. (1b), which shows the temperature distribution at the cross-interface using PWCM. The horizontal dashed line corresponds to the temperature distribution by using SM. It is known that the SM cannot present a specific image of temperature distribution, i.e., black box. In SM, it is considered that the total thermal resistance is a simple series connection of intrinsic thermal resistance and interfacial thermal resistance. As for PWCM, it can provide a clear physical image of temperature distribution and reveal the mechanism of the two-dimensional thermal transport at the cross-interface. By using PWCM, the total thermal resistance is represented by a series of intrinsic thermal resistance and interfacial thermal resistance with a specific interacting relationship.

In order to assess the accuracy of PWCM, $R_{\text{inter\_SM}}$, $R_{\text{inter\_PWCM}}$, and $R_{\text{inter\_exact}}$, which are the interfacial thermal resistances calculated by SM, PWCM, and average temperature difference method, respectively, are compared in Fig. 4(b). Here, to make the description and comparison of variables more intuitionistic, suffix is added to the subscript of the variable R_{inter} to distinguish the values calculated by these three methods. $R_{\text{inter\_SM}}$ denotes the inter-ribbon thermal resistance calculated by the simplified model. $R_{\text{inter\_PWCM}}$ denotes the inter-ribbon thermal resistance calculated by the phonon weak couplings model. $R_{\text{inter\_exact}}$ denotes the inter-ribbon thermal resistance calculated by the ratio of the temperature difference to the heat flux.

Based on idea of experimental measurements, $R_{\text{inter\_SM}}$ is calculated by the difference between $R_{\text{total\_SM}}$ and $R_{\text{intra\_SM}}$. The formula using the SM can be given as

$$\begin{aligned} R_{\text{inter\_SM}} &= R_{\text{total\_SM}} - R_{\text{intra\_SM}} \\ &= \frac{T_{\text{T}}|_{x=0} - T_{\text{B}}|_{x=L_{\text{C}}}}{J} - \frac{L_{\text{C}}}{2\kappa_0 A}, \end{aligned} \tag{8}$$

where κ_0 is the thermal conductivity of bare GNR which means no CC is bonded between the GNRs. As for $R_{\text{inter\_exact}}$, it is calculated by the ratio of the temperature difference to the heat flux which is recognized as an accurate calculation formula for solving the interfacial thermal conductivity:[47,51,55]

$$G_{\text{CA}} = \frac{J}{w(\bar{T}_{\text{T}} - \bar{T}_{\text{B}})L_{\text{C}}}, \tag{9a}$$

$$R_{\text{inter\_exact}} = \frac{1}{G_{\text{CA}} w L_{\text{C}}}, \tag{9b}$$

where $\bar{T}_{\text{T}}$ and $\bar{T}_{\text{B}}$ denote the average temperatures of T_{T} and T_{B}, respectively. It is noteworthy that although $R_{\text{inter\_PWCM}}$ and $R_{\text{inter\_exact}}$ are both calculated by the idea of average temperature difference, the average temperature in $R_{\text{inter\_PWCM}}$ is calculated by integral of the fitted function while that in $R_{\text{inter\_exact}}$ is obtained through arithmetic mean of temperature data in the overlapped region. Thus, a significant advantage of PWCM over the average temperature difference method is that the theoretical equation of temperature distribution in the overlapped area can be obtained, which will help explore the mechanism of interfacial thermal transport.

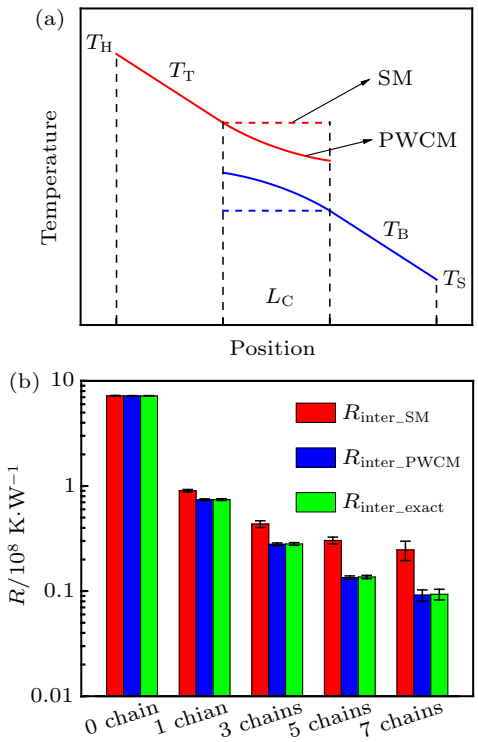

Fig. 4. (a) Theoretical curve of temperature distribution using PWCM and SM. (b) The comparison of the interfacial thermal resistance calculated by SM, PWCM, and average temperature difference, i.e., $R_{\text{inter\_SM}}$ (red bar), $R_{\text{inter\_PWCM}}$ (blue bar), and $R_{\text{inter\_exact}}$ (green bar), respectively, in five cases with different numbers of carbon chains.

From Fig. 4(b), it can be seen that $R_{\text{inter\_PWCM}}$ always remains almost consistent with $R_{\text{inter\_exact}}$, however $R_{\text{inter\_SM}}$ appears some deviation compared with $R_{\text{inter\_exact}}$, especially when the number of CCs increases more. The reason is that when CC is bonded, the thermal conductivity of the GNR in the system is no longer equal to that of bare GNR (i.e., κ_0). However, based on the idea of SM, the thermal conductivity of bare GNR is still applied to calculate the $R_{\text{inter\_SM}}$ and the deviation will be more obvious when more CCs are bonded. For PWCM, it can exhibit the two-dimensional thermal transport process and obtain a clear temperature distribution profile which make it possible to directly calculate $R_{\text{inter\_PWCM}}$ accurately. Therefore, the accuracy of PWCM relative to SM is verified in the example of overlapped GNRs. Furthermore, the PWCM can be used to better guide how to reduce the interface thermal resistance of graphene-based composites by adding the bonded carbon chains.

4. Conclusion

In summary, the interfacial thermal resistance between overlapped graphene nanoribbons is reduced by bonding carbon chains through NEMD simulation, and the phonon weak couplings model is applied to analyze and explain the interfacial thermal transport mechanism. After one CC is bonded, the interfacial thermal resistance is reduced by an order of magnitude because the covalent bond interactions largely enhance the interfacial thermal transport. When more CCs are bonded, the decreasing rate of the interfacial thermal resistance slows down gradually, which can be explained by the proposed numerical relationship between thermal resistance and number of CCs based on PWCM, i.e., $R_{\text{inter}} \propto 1/\sqrt{N}$. Moreover, the advantage of PWCM relative to the traditional simplified model is demonstrated in the example of overlapped GNRs especially when more CCs are bonded. This work can provide a valuable guide for the design and application of graphene-based materials for effective thermal management and modulation.

Acknowledgements

We are grateful to Xiao Wan and Shichen Deng for their useful discussions. The authors thank the National Supercomputing Center in Tianjin (NSCC-TJ) and High Performance Computer Cluster in Huazhong University of Science and Technology (HUST-HPCC) for providing assistance with computations.

References

[1] Zhang Z and Chen J 2018 *Chin. Phys. B* **27** 035101
[2] Gu X, Wei Y, Yin X, Li B and Yang R 2018 *Rev. Mod. Phys.* **90** 041002
[3] Zhang Z, Ouyang Y, Cheng Y, Chen J, Li N and Zhang G 2020 *Phys. Rep.* **860** 1
[4] Xie Q, Wang L, Li J, Li R and Chen X Q 2020 *Chin. Phys. B* **29** 037306
[5] Balandin A A, Ghosh S, Bao W, Calizo I, Teweldebrhan D, Miao F and Lau C N 2008 *Nano Lett.* **8** 902
[6] Balandin A A 2011 *Nat. Mater.* **10** 569
[7] Yang N, Xu X, Zhang G and Li B 2012 *AIP Adv.* **2** 041410
[8] Xu X, Pereira L F, Wang Y, Wu J, Zhang K, Zhao X, Bae S, Bui C T, Xie R and Thong J T 2014 *Nat. Commun.* **5** 3689
[9] Cheng Z F and Zheng R L 2016 *Chin. Phys. Lett.* **33** 046501
[10] Lee C, Wei X, Kysar J W and Hone J 2008 *Science* **321** 385
[11] Novoselov K S, Fal V, Colombo L, Gellert P, Schwab M and Kim K 2012 *Nature* **490** 192
[12] Tsen A W, Brown L, Levendorf M P, Ghahari F, Huang P Y, Havener R W, Ruiz-Vargas C S, Muller D A, Kim P and Park J 2012 *Science* **336** 1143
[13] Cao Y, Fatemi V, Fang S, Watanabe K, Taniguchi T, Kaxiras E and Jarillo-Herrero P 2018 *Nature* **556** 43
[14] Novoselov K S, Geim A K, Morozov S V, Jiang D, Zhang Y, Dubonos S V, Grigorieva I V and Firsov A A 2004 *Science* **306** 666
[15] Zhang N, Liu B and Lin L W 2020 *Acta Phys. Sin.* **69** 016101 (in Chinese)
[16] Lin Q M, Zhang X, Lu Q C, Luo Y B, Cui J G, Yan X, Ren X M and Huang X 2019 *Acta Phys. Sin.* **68** 247302 (in Chinese)
[17] Guo W L, Deng J, Wang J L, Wang L and Tai J P 2019 *Acta Phys. Sin.* **68** 247303 (in Chinese)
[18] Nair R R, Blake P, Grigorenko A N, Novoselov K S, Booth T J, Stauber T, Peres N M and Geim A K 2008 *Science* **320** 1308
[19] Falkovsky L 2008 *J. Phys.: Conf. Ser.* **129** 012004
[20] Chen J, Walther J H and Koumoutsakos P 2015 *Adv. Funct. Mater.* **25** 7539
[21] Alexeev D, Chen J, Walther J H, Giapis K P, Angelikopoulos P and Koumoutsakos P 2015 *Nano Lett.* **15** 5744
[22] Han H, Zhang Y, Wang N, Samani M K, Ni Y, Mijbil Z Y, Edwards M, Xiong S, Sääskilahti K and Murugesan M 2016 *Nat. Commun.* **7** 11281
[23] Chen J, Walther J H and Koumoutsakos P 2014 *Nano Lett.* **14** 819
[24] Pereira L F C and Donadio D 2013 *Phys. Rev. B* **87** 125424
[25] Chen J, Walther J H and Koumoutsakos P 2016 *Nanotechnology* **27** 465705
[26] Pop E, Varshney V and Roy A K 2012 *MRS Bull.* **37** 1273
[27] Chen S, Wang Q, Zhang M, Huang R, Huang Y, Tang J and Liu J 2020 *Carbon* **167** 270
[28] Xie Y, Yuan P, Wang T, Hashemi N and Wang X 2016 *Nanoscale* **8** 17581
[29] Lin S, Anwer M A, Zhou Y, Sinha A, Carson L and Naguib H E 2018 *Composites, Part B* **132** 61
[30] Guo H, Li X, Li B, Wang J and Wang S 2017 *Mater. Des.* **114** 355
[31] Luo T and Lloyd J R 2012 *Adv. Funct. Mater.* **22** 2495
[32] Chi C, Li Y, Li D, Huang H, Wang Q, Yang Y and Huang B 2019 *J. Mater. Chem. A* **7** 16748
[33] Wang N, Samani M K, Li H, Dong L, Zhang Z, Su P, Chen S, Chen J, Huang S and Yuan G 2018 *Small* **14**
[34] Peng L, Xu Z, Liu Z, Guo Y, Li P and Gao C 2017 *Adv. Mater.* **29** 1700589
[35] Zhao W, Chen W, Yue Y and Wu S 2017 *Appl. Therm. Eng.* **113** 481
[36] Gao J, Meng C, Xie D, Liu C, Bao H, Yang B, Li M and Yue Y 2019 *Appl. Therm. Eng.* **150** 1252
[37] Shahil K M and Balandin A A 2012 *Solid State Commun.* **152** 1331
[38] Huang H, Liu C, Wu Y and Fan S 2005 *Adv. Mater.* **17** 1652
[39] Zhu H, Li Y, Fang Z, Xu J, Cao F, Wan J, Preston C, Yang B and Hu L 2014 *ACS nano* **8** 3606
[40] Shen B, Zhai W and Zheng W 2014 *Adv. Funct. Mater.* **24** 4542
[41] Zhang J, Shi G, Jiang C, Ju S and Jiang D 2015 *Small* **11** 6197
[42] Malekpour H, Chang K H, Chen J C, Lu C Y, Nika D, Novoselov K and Balandin A 2014 *Nano Lett.* **14** 5155
[43] Ju S, Shiga T, Feng L, Hou Z, Tsuda K and Shiomi J 2017 *Phys. Rev. X* **7** 021024
[44] Zhang H, Xiong S, Wang H, Volz S and Ni Y 2019 *EPL* **125** 46001
[45] Tian Z, Esfarjani K and Chen G 2012 *Phys. Rev. B* **86** 235304
[46] Yang Y, Chen H, Wang H, Li N and Zhang L 2018 *Phys. Rev. E* **98** 042131
[47] Deng C, Yu X, Huang X and Yang N 2017 *J. Heat Transfer* **139**
[48] Sun F, Zhang T, Jobbins M M, Guo Z, Zhang X, Zheng Z, Tang D, Ptasinska S and Luo T 2014 *Adv. Mater.* **26** 6093
[49] Yue Y, Zhang J, Xie Y, Chen W and Wang X 2017 *Int. J. Heat Mass Transfer* **110** 827

[50] Qiu L, Zou H, Wang X, Feng Y, Zhang X, Zhao J, Zhang X and Li Q 2019 *Carbon* **141** 497
[51] Liu X, Zhang G and Zhang Y-W 2014 *J. Phys. Chem. C* **118** 12541
[52] Xu Z and Buehler M J 2009 *ACS nano* **3** 2767
[53] Yang J, Waltermire S, Chen Y, Zinn A A, Xu T T and Li D 2010 *Appl. Phys. Lett.* **96** 023109
[54] Yang J, Shen M, Yang Y, Evans W J, Wei Z, Chen W, Zinn A A, Chen Y, Prasher R and Xu T T 2014 *Phys. Rev. Lett.* **112** 205901
[55] Zhong H and Lukes J R 2006 *Phys. Rev. B* **74** 125403
[56] Shi L, Li D, Yu C, Jang W, Kim D, Yao Z, Kim P and Majumdar A 2003 *J. Heat Transfer* **125** 881
[57] Tang H, Wang X, Xiong Y, Zhao Y, Zhang Y, Zhang Y, Yang J and Xu D 2015 *Nanoscale* **7** 6683
[58] Deng C, Huang Y, An M and Yang N 2021 *Mater. Today Phys.* **16** 100305
[59] Xiong Y, Yu X, Huang Y, Yang J, Li L, Yang N and Xu D 2019 *Mater. Today Phys.* **11** 100139
[60] Feng W, Yu X, Wang Y, Ma D, Sun Z, Deng C and Yang N 2019 *Phys. Chem. Chem. Phys.* **21** 25072
[61] Chen G 2005 *Nanoscale energy transport and conversion: a parallel treatment of electrons, molecules, phonons, and photons* (Oxford: Oxford University Press)
[62] Ma D, Arora A, Deng S, Xie G, Shiomi J and Yang N 2019 *Mater. Today Phys.* **8** 56
[63] An M, Song Q, Yu X, Meng H, Ma D, Li R, Jin Z, Huang B and Yang N 2017 *Nano Lett.* **17** 5805
[64] Ma D, Wan X and Yang N 2018 *Phys. Rev. B* **98** 245420
[65] Wan X, Feng W, Wang Y, Wang H, Zhang X, Deng C and Yang N 2019 *Nano Lett.* **19** 3387
[66] Xing L and Wei Rong Z 2015 *Chin. Phys. Lett.* **32** 096501
[67] Hu S, Chen J, Yang N and Li B 2017 *Carbon* **116** 139
[68] Ma D, Ding H, Wang X, Yang N and Zhang X 2017 *Int. J. Heat Mass Transfer* **108** 940
[69] Swope W C, Andersen H C, Berens P H and Wilson K R 1982 *The Journal of chemical physics* **76** 637
[70] Plimpton S 1995 *J. Comput. Phys.* **117** 1
[71] Cui L, Feng Y, Tang J, Tan P and Zhang X 2016 *Int. J. Therm. Sci.* **99** 64
[72] Xie G, Ding D and Zhang G 2018 *Adv. Phys. X* **3** 1480417
[73] Ding Z, An M, Mo S, Yu X, Jin Z, Liao Y, Esfarjani K, LJ̈ T, Shiomi J and Yang N 2019 *J. Mater. Chem. A* **7** 2114
[74] Guo Z, Zhang D and Gong X G 2009 *Appl. Phys. Lett.* **95** 163103